Bulletin of Mathematical Biology (2020) 82:3
https://doi.org/10.1007/s11538-019-00676-z

Society for Mathematical Biology

ORIGINAL ARTICLE

Surfing the Hyperbola Equations of the Steady-State Farquhar–von Caemmerer–Berry C_3 Leaf Photosynthesis Model: What Can a Theoretical Analysis of Their Oblique Asymptotes and Transition Points Tell Us?

Jon Miranda-Apodaca[1] · **Emilio L. Marcos-Barbero**[1] · **Rosa Morcuende**[1] · **Juan B. Arellano**[1]

Received: 9 August 2019 / Accepted: 2 December 2019 / Published online: 23 December 2019

Abstract

The asymptotes and transition points of the net CO_2 assimilation (A/C_i) rate curves of the steady-state Farquhar–von Caemmerer–Berry (FvCB) model for leaf photosynthesis of C_3 plants are examined in a theoretical study, which begins from the exploration of the standard equations of hyperbolae after rotating the coordinate system. The analysis of the A/C_i quadratic equations of the three limitation states of the FvCB model—abbreviated as A_c, A_j and A_p—allows us to conclude that their oblique asymptotes have a common slope that depends only on the mesophyll conductance to CO_2 diffusion (g_m). The limiting values for the transition points between any two states of the three limitation states c, j and p do not depend on g_m, and the results are therefore valid for rectangular and non-rectangular hyperbola equations of the FvCB model. The analysis of the variation of the slopes of the asymptotes with g_m casts doubts about the fulfilment of the steady-state conditions, particularly, when the net CO_2 assimilation rate is inhibited at high CO_2 concentrations. The application of the theoretical analysis to extended steady-state FvCB models, where the hyperbola equations of A_c, A_j and A_p are modified to accommodate nitrogen assimilation and amino acids export via the photorespiratory pathway, is also discussed.

Keywords FvCB model · Mesophyll conductance · Leaf photosynthesis · Net CO_2 assimilation rate · Resistance to CO_2 diffusion · Rubisco

Electronic supplementary material The online version of this article (https://doi.org/10.1007/s11538-019-00676-z) contains supplementary material, which is available to authorized users.

✉ Juan B. Arellano
juan.arellano@irnasa.csic.es

[1] Departamento de Estrés Abiótico, Instituto de Recursos Naturales y Agrobiología de Salamanca (IRNASA-CSIC), Cordel de Merinas, 40-52, 37008 Salamanca, Spain

1 Introduction

The steady-state Farquhar–von Caemmerer–Berry (FvCB) leaf photosynthesis model is broadly recognised by plant biologists and physiologists as one of the most useful models to assess in vivo the net CO_2 assimilation rate (A) of plant leaves as a function of CO_2 concentration (C) under different environmental cues. The initial FvCB model was first described in the 1980s for C_3 plants (Farquhar et al. 1980), then modified to include the triose phosphate utilisation (Sharkey 1985a, b) and later extended to other works on C_4 plants, antisense transgenic plants, the effect of bicarbonate pumps at the chloroplast envelope and global climate change, among others (Bellasio et al. 2016; Price et al. 2011; von Caemmerer 2000; Wullschleger 1993). Together with the basic rectangular hyperbolic FvCB model (Farquhar et al. 1980; Sharkey 1985a, b), other non-rectangular hyperbolic, exponential and empirical steady-state models have also been described (Duursma 2015; Ethier and Livingston 2004; Goudriaan 1979; von Caemmerer 2000). In the basic FvCB model, the steady-state CO_2 assimilation rate proceeds at the minimum of three limitation rates denoted as A_c, A_j and A_p, which depend on the activity of the ribulose-1,5-bisphosphate carboxylase/oxygenase (Rubisco), the ribulose-1,5-bisphosphate regeneration and the triose phosphate utilisation, hereafter abbreviated as states c, j and p.

In the basic FvCB model, the analysis of the net CO_2 assimilation rate did not consider the (apparent) mesophyll conductance to CO_2 diffusion (g_m)—hereafter defined as the conductance for CO_2 diffusion from the intercellular space to the site of Rubisco carboxylation assuming that photorespiratory and respiratory CO_2 release occurs in the same compartment as Rubisco carboxylation (von Caemmerer 2013)—and thus, its value was assumed to be infinite. Consequently, the CO_2 concentration in the intercellular (or substomatal) space (C_i) was set equal to the CO_2 concentration at the site of Rubisco carboxylation (C_c) and both rate curves, A/C_c and A/C_i, were not distinguished between each other. The inclusion of a finite value for g_m into the initial FvCB model transforms A_c and A_j into quadratic equations. This transformation was indeed demonstrated to provide a more accurate estimation of the values for the maximum carboxylation rate (V_{cmax}) of Rubisco and the maximum electron transport J_{max} under steady-state conditions (Ethier and Livingston 2004; Niinemets et al. 2009; von Caemmerer 2000). From a mathematical point of view, the main difference between the equations of the A/C_c and A/C_i rate curves is that the latter are non-rectangular hyperbolae, whose curvature shape in the first quadrant of the Cartesian coordinate system depends on the magnitude of g_m.

Nowadays, A/C_i, instead of A/C_c, rate curves are extensively used in the estimation of biochemical parameters from leaf photosynthesis, where g_m is assumed to be finite and purely diffusional and not to depend on the CO_2 concentration inside the leaf. However, the assumption that g_m remains constant has been challenged in some studies and new extensions have been incorporated into the FvCB model (Flexas et al. 2007; Tholen et al. 2012). For instance, g_m was proposed to depend on the ratio of mitochondrial CO_2 release to chloroplast CO_2 uptake

and to decrease particularly at low C_i (Tholen et al. 2012), although other factors, such as the intracellular arrangements of chloroplasts and mitochondria in C_3 leaves, were later included in a more generalised model to better explain the dependence of g_m on the above ratio (Yin and Struik 2017). A decrease in the values for g_m was also observed in response to an increase in C_i (Flexas et al. 2007). In this latter study, either modifications in chloroplast shape, which could prevent the chloroplast association with the cell surface, or the involvement of aquaporins, which could facilitate CO_2 diffusion across cell membranes by a pH-dependent process, was proposed to regulate the variation of g_m. Besides, g_m is tightly co-regulated with the stomatal conductance (g_s) (Flexas et al. 2008). g_s varies with both the atmospheric CO_2 concentration and the limitation state (Buckley 2017). The value of g_s declines with increased atmospheric CO_2 concentration under RuBP regeneration-limited photosynthesis, but, in contrast, it increases with increased atmospheric CO_2 concentration under Rubisco-limited photosynthesis (Medlyn et al. 2011).

When the A/C_i rate curves of the FvCB model are analysed under steady-state conditions and the photorespiratory and respiratory CO_2 release is also assumed to take place at the site of the Rubisco carboxylation, the quadratic equations for A_c, A_j and A_p (see "Appendix 1", Eqs. A8–A10) can be fitted following different approaches, where g_m is taken as a constant parameter (Duursma 2015; Gu et al. 2010; Sharkey 2016; Su et al. 2009). Some of the nonlinear fitting methods require starting from initial guessed parameters and letting the fit improve with successive iterations, while others constrain the C_i values at which the transition point between c and j occurs. A wealth of data on the transition point between the states c and j indicates that its value is species- and season-dependent, and so it should not be constrained in the fitting method (Duursma 2015; Miao et al. 2009; Zeng et al. 2010). The above fitting methods also take up that the A/C_i rate curves reach asymptotic values for A at supraoptimal CO_2 concentration, when there is experimental evidence for the inhibition of the net CO_2 assimilation rate by CO_2 itself at high concentrations (Woo and Wong 1983). Also, some of these fitting methods make use of approximate estimations for J_{max} and T_p—where T_p stands for the rate of phosphate release in triose phosphate utilisation—when C_c approaches infinity in an A/C_c rate curve (Su et al. 2009) or they reasonably assume that the order of the three limitation states along the C_i axis is the same as along the C_c axis (Gu et al. 2010). Dynamic models of photosynthesis are also suitable to analyse the leaf CO_2 assimilation response under fluctuating environmental stimuli such as sunlight irradiance, atmospheric CO_2 concentration or stomatal response to light (Bellasio 2019; Morales et al. 2018; Noe and Giersch 2004); however, they add complexity to the analysis or they have not been developed completely to date.

The simplicity of the quadratic equations for A_c, A_j and A_p still makes the steady-state FvCB model very useful in fitting approaches to estimate biochemical parameters from leaf photosynthesis (Duursma 2015; Gu et al. 2010; Sharkey 2016; Su et al. 2009). After nearly 40 years of research on the FvCB model, its quadratic equations still hide mathematical features of interest to establish when this model becomes short or when an extended FvCB model would be more suitable for the estimation of the biochemical parameters. On the mathematical analysis of the

FvCB model we present here, the rotation of the coordinate system has been a key strategy to reach the conclusion that the quadratic equations of the FvCB model cannot explain the inhibition of the net CO_2 assimilation rate at very high C_i. Also, the mathematical analysis of the limiting conditions for the transition points between A_c, A_j and A_p shows that they do not depend on the finite value of g_m.

2 Computer Analysis

The computer algebra system Wolfram Mathematica v. 10.3 (Wolfram Research 2015) was used to program scripts to solve analytically the asymptotes and transition points of A/C_c and A/C_i rate curves of the three limitation states c, j and p. Comparative analyses were performed with hyperbolae in standard form after the rotation of the coordinates. The scripts were also run to plot representative A/C_c and A/C_i rate curves. The chosen and finite values for the kinetic constants for Rubisco and other biochemical parameters in the simulations are in the range of those experimentally determined for different C_3 plant species (Jahan et al. 2014; von Caemmerer 2000). A list of definitions is given in Table 1 for the sake of clarity.

3 Results and Discussion

3.1 Brief Description of the Asymptotes and Transition Points of the Rectangular Hyperbola Equations of the Basic FvCB Model

According to the basic FvCB model for leaf photosynthesis in C_3 plants (Farquhar et al. 1980; Sharkey 1985a, b), the hyperbola equations of the dependence of the net CO_2 assimilation rate on the CO_2 concentration at the site of the Rubisco carboxylation (i.e. A/C_c) are as follows:

$$A = V_c(1 - 0.5\phi) - R_d = \min\{A_c, A_j, A_p\} \tag{1}$$

with

$$A_c = \frac{V_{cmax}(C_c - \Gamma^*)}{C_c + K_{co}} - R_d, \tag{2}$$

$$A_j = \frac{J(C_c - \Gamma^*)}{4C_c + 8\Gamma^*} - R_d, \tag{3}$$

$$A_p = \frac{3T_p(C_c - \Gamma^*)}{C_c - (1 + 3\alpha)\Gamma^*} - R_d, \tag{4}$$

where A proceeds at a minimum of the three limitation rates A_c, A_j and A_p. The equations of the three rate curves in the basic FvCB model are branches of rectangular

Table 1 List of biochemical parameters used with their definition and units

Symbol	Definition	Units
A	Net CO_2 assimilation rate	μmol m^{-2} s^{-1}
A_c	Net CO_2 assimilation rate assuming Rubisco limitation	μmol m^{-2} s^{-1}
A_j	Net CO_2 assimilation rate assuming ribulose-1,5-bisphosphate regeneration limitation	μmol m^{-2} s^{-1}
A_p	Net CO_2 assimilation rate assuming triose phosphate use limitation	μmol m^{-2} s^{-1}
A_{*1}^{xy}	A at the transition point between any two limitation states (x and y) of the three states c, j and p in the fourth (or third) quadrant of the Cartesian coordinate system. The symbol * stands for chloroplast space (c), intercellular (i) or atmosphere (a)	μmol m^{-2} s^{-1}
A_{*2}^{xy}	As A_{*1}^{xy}, except that the transition point takes place in the first quadrant of the Cartesian coordinate system.	μmol m^{-2} s^{-1}
C_c	Chloroplast CO_2 concentration	Pa
C_i	Intercellular CO_2 concentration	Pa
C_a	Atmospheric CO_2 concentration	Pa
C_{*1}^{xy}	CO_2 concentration at the transition point between any two limitation states (x and y) of the three states c, j and p in the fourth (or third) quadrant of the Cartesian coordinate system. * stands for chloroplast (c), intercellular space (i) or atmosphere (a)	Pa
C_{*2}^{xy}	As C_{*1}^{xy}, except the transition point takes place in the first quadrant of the Cartesian coordinate system	Pa
$C_{c2\to1}^{xy}$	Value of the CO_2 concentration when C_{c2}^{xy} approaches C_{c1}^{xy}	Pa
$C_{c2\to\infty}^{xy}$	Value of the CO_2 concentration when C_{c2}^{xy} approaches infinity	Pa
$C_{i2\to1}^{xy}$	Value of the CO_2 concentration when C_{i2}^{xy} approaches C_{i1}^{xy}	Pa
$C_{i2\to\infty}^{xy}$	Value of the CO_2 concentration when C_{i2}^{xy} approaches infinity	Pa
J	Electron transport rate	μmol m^{-2} s^{-1}
J_{max}	Maximal electron transport rate	μmol m^{-2} s^{-1}
K_c	Rubisco Michaelis–Menten constant for carboxylation	Pa
K_o	Rubisco Michaelis–Menten constant for oxygenation	Pa
K_{co}	Apparent Michaelis–Menten constant	Pa
O	Oxygen concentration	Pa
R_d	Respiration rate in the light	μmol m^{-2} s^{-1}

Table 1 (continued)

Symbol	Definition	Units
r_m	Apparent mesophyll resistance to CO_2 diffusion (see the Introduction section). Inverse of g_m	Pa μmol^{-1} m^2 s
r_s	Stomatal resistance to CO_2 diffusion. Inverse of g_s	Pa μmol^{-1} m^2 s
T_p	Triose phosphate export rate from chloroplasts	μmol m^{-2} s^{-1}
V_{cmax}	Maximum carboxylation rate	μmol m^{-2} s^{-1}
y^x_{asyn}	Asymptote with horizontal slope of A_x, where x stands for c, j or p	μmol m^{-2} s^{-1}Pa^{-1}
y^x_{asyp}	Asymptote with positive slope of A_x, where x stands for c, j or p	μmol m^{-2} s^{-1}Pa^{-1}
α	Fraction of glycerate that does not return to chloroplasts through the photorespiratory cycle	Dimensionless
β	Angle of rotation of the coordinate system	Dimensionless
Γ^*	Chloroplast CO_2 photocompensation point	Pa

hyperbolae opening upwards and downwards or left and right, where the coordinate system has been rotated 45° (Appendix 1). The two asymptotes of each of the hyperbolic equations (Eqs. 2–4) are perpendicular to each other with slopes 0 and infinite (Table 2). An elemental analysis of the transition points between the rate equations of the three limitation states gives the following sets of solutions:

For $A_c = A_j$,

$$C_{c1}^{cj} = \Gamma^* \quad \text{and} \quad A_{c1}^{cj} = -R_d, \tag{5a, 5b}$$

$$C_{c2}^{cj} = \frac{8V_{cmax}\Gamma^* - JK_{co}}{J - 4V_{cmax}} \quad \text{and} \quad A_{c2}^{cj} = \frac{(J - 4R_d)K_{co} + (J + 8R_d - 12V_{cmax})\Gamma^*}{4K_{co} - 8\Gamma^*} \tag{6a, 6b}$$

for $A_j = A_p$,

$$C_{c1}^{jp} = \Gamma^* \quad \text{and} \quad A_{c1}^{jp} = -R_d, \tag{7a, 7b}$$

$$C_{c2}^{jp} = \frac{(J + 24T_p + 3\alpha J)\Gamma^*}{J - 12T_p} \quad \text{and} \quad A_{c2}^{jp} = \frac{12T_p + \alpha J - 4R_d(1 + \alpha)}{4(1 + \alpha)}, \tag{8a, 8b}$$

and for $A_c = A_p$,

$$C_{c1}^{cp} = \Gamma^* \quad \text{and} \quad A_{c1}^{cp} = -R_d, \tag{9a, 9b}$$

$$C_{c2}^{cp} = \frac{(1 + \alpha)V_{cmax}\Gamma^* + 3T_pK_{co}}{V_{cmax} - 3T_p} \quad \text{and} \tag{10a}$$

$$A_{c2}^{cp} = \frac{(3(T_p + \alpha V_{cmax}) - (1 + \alpha)R_d)\Gamma^* + (3T_p - R_d)K_{co}}{K_{co} + (1 + \alpha)\Gamma^*} \tag{10b}$$

Together with the transition points $(C_{c2}^{xy}, A_{c2}^{xy})$ between any two limitation states of the three states c, j and p (superscripts x and y) in the first quadrant of the Cartesian coordinate system (subscript 2), there is a common transition point $(C_{c1}^{xy}, A_{c1}^{xy})$ in the fourth quadrant (subscript 1) when $\alpha \neq 0$ $(0 \leq \alpha \leq 1)$. Carbon and electron requirements for the assimilation of nitrogen and export of amino acids through the photorespiratory pathway (Busch et al. 2018) are not addressed here, and the standard definition for α in the basic FvCB model remains (see below for further discussion).

3.2 Dependence of the Oblique Asymptotes of the Non-rectangular Hyperbola (or Quadratic) Equations of the FvCB Model on r_m

The mathematical analysis becomes more challenging if A/C_i, instead of A/C_c, rate curves are used. When steady-state conditions for CO_2 diffusion are achieved, A_c, A_j and A_p can be determined after the substitution of C_c for C_i using the equation

Table 2 Summary of the values and equations of the centre, asymptotes and bisecting lines describing the rectangular and non-rectangular hyperbolae of the FvCB model for C_3 plants

	Vertical asymptote	Horizontal asymptote	Centre	Bisecting line
Rectangular hyperbolae				
A_c	$C_i^c = -K_{co}$	$A_{asyn}^c = V_{cmax} - R_d$	$\left(-K_{co}, V_{cmax} - R_d\right)$	$A_{bis}^c = -\left(C_i + K_{co}\right) + V_{cmax} - R_d$
A_j	$C_i^j = -2\Gamma^*$	$A_{asyn}^j = J/4 - R_d$	$\left(-2\Gamma^*, J/4 - R_d\right)$	$A_{bis}^j = -\left(C_i + 2\Gamma^*\right) + J/4 - R_d$
A_p	$C_i^p = (1+3\alpha)\Gamma^*$	$A_{asyn}^p = 3T_p - R_d$	$\left((1+3\alpha)\Gamma^*, 3T_p - R_d\right)$	$A_{bis}^p = \left(C_i - (1+3\alpha)\Gamma^*\right) + 3T_p - R_d$
	Oblique asymptote	Horizontal asymptote	Centre	Bisecting line
Non-rectangular hyperbolae				
A_c	$A_{asyp}^c = \frac{C_i + K_{co}}{r_m}$	$A_{asyn}^c = V_{cmax} - R_d$	$\left(\left(V_{cmax} - R_d\right)r_m - K_{co}, V_{cmax} - R_d\right)$	$A_{bis}^c = -\left(r_m + \sqrt{1+r_m^2}\right)\left(C_i - (V_{cmax} - R_d)r_m + K_{co}\right) + V_{cmax} - R_d$
A_j	$A_{asyp}^j = \frac{C_i + 2\Gamma^*}{r_m}$	$A_{asyn}^j = J/4 - R_d$	$\left(\left(J/4 - R_d\right)r_m - 2\Gamma^*, J/4 - R_d\right)$	$A_{bis}^j = -\left(r_m + \sqrt{1+r_m^2}\right)\left(C_i - \left(J/4 - R_d\right)r_m + 2\Gamma^*\right) + J/4 - R_d$
A_p	$A_{asyp}^p = \frac{C_i - (1+3\alpha)\Gamma^*}{r_m}$	$A_{asyn}^p = 3T_p - R_d$	$\left(\left(3T_p - R_d\right)r_m + (1+3\alpha)\Gamma^*, 3T_p - R_d\right)$	$A_{bis}^p = \left(-r_m + \sqrt{1+r_m^2}\right)\left(C_i - \left(3T_p - R_d\right)r_m - (1+3\alpha)\Gamma^*\right) + 3T_p - R_d$

$A = (C_i - C_c)/r_m$ according to Fick's diffusion law, where the finite and "constant" mesophyll resistance to CO_2 diffusion is $r_m = 1/g_m$. Quadratic equations are obtained for A_c, A_j and A_p (Eqs. A8–A10). They are now non-rectangular hyperbolae opening upwards and downwards, for the case of A_c and A_j, and left and right, for the case of A_p, where the coordinate system has now been rotated anticlockwise an angle, here denoted β (Appendix 1). One of the two asymptotes from each non-rectangular hyperbola is parallel to the horizontal axis, but the other is now oblique with a slope exactly equal to the mesophyll conductance to CO_2 diffusion, i.e. $g_m = 1/r_m$, a result which is valid for A_c (von Caemmerer 2000) and also for A_j and A_p. This conclusion is reached following the analysis of the coefficients of the quadratic equations obtained after the anticlockwise rotation of the coordinate system by β. When Eqs. A6 and A7 are compared with Eqs. A8–A10, some key features emerge: firstly, the summation of the coefficients of C_i^2 is equal to zero and, secondly, the second coefficient of the quadratic equations is, in fact, the summation of the two asymptotes of each hyperbola (Appendix 1). The equations of the two asymptotes for A_c, A_j and A_p are therefore summarised as follows:

$$y^c_{asyp} = \frac{C_i + K_{co}}{r_m} \quad \text{and} \quad y^c_{asyn} = V_{cmax} - R_d, \tag{11a, 11b}$$

$$y^j_{asyp} = \frac{C_i + 2\Gamma^*}{r_m} \quad \text{and} \quad y^j_{asyn} = J/4 - R_d, \text{ and} \tag{12a, 12b}$$

$$y^p_{asyp} = \frac{C_i - (1 + 3\alpha)\Gamma^*}{r_m} \quad \text{and} \quad y^p_{asyn} = 3T_p - R_d, \tag{13a, 13b}$$

where y^x_{asyp} and y^x_{asyn} stand for the oblique and horizontal asymptotes of A_c, A_j and A_p, respectively.

It is worth noting that the use of $\alpha = 0$ directly in Eq. 4 is an oversimplification of A_p. The oblique asymptote of A_p is present, even when α is assumed to be equal to zero (Eq. 13a). The intersection between the two asymptotes of A_p (i.e. y^p_{asyp} and y^p_{asyn}), in particular when $\alpha = 0$, gives a limiting value below which C_i is meaningless. In fact, the approximation $A_p = 3T - R_d$ is not valid in the whole C_i domain between $\Gamma^* \le C_i \le \infty$. The discontinuity is more obvious when $\alpha \neq 0$ because there is a C_i domain for which no real values for A_p can be obtained. The suitable C_i domain for the nonlinear fitting of A_p in the FvCB model is thus confined to the negative root of its branch opening right (Fig. 1), a result which is also in line with the study by Gu et al. (2010). When $\alpha \neq 0$, the values of the negative root of the A_p branch opening right decrease as C_i increases.

3.3 The Limiting Conditions for the Transition Points in the FvCB Model Do Not Depend on r_m

The transition points for the negative roots of the quadratic equations for A/C_i (Eqs. A8–A10) can be solved mathematically and written in a simple form making use of the analytical solutions (Eqs. 5–10) for A/C_c as follows:

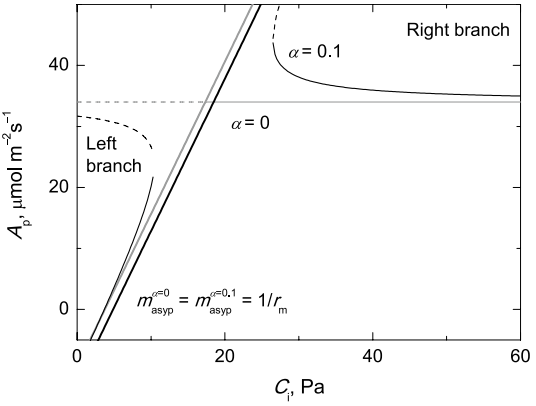

Fig. 1 Representative A_p rate curves for the non-rectangular FvCB model for C_3 plants with two different values for α and their corresponding oblique asymptotes. The negative root (thin solid line) and the positive root (thin dashed line) of the quadratic equation of A_p together with its oblique asymptote (thick solid line) are in grey for $\alpha = 0$. The negative root (thin solid line) and the positive root (thin dashed line) of the quadratic equation of A_p together with its oblique asymptote (thick solid line) are in black for $\alpha = 0.1$. The simulation was performed using the following values for the biochemical parameters: T_p, 12 μmol m^{-2} s^{-1}; R_d, 2 μmol m^{-2} s^{-1}; r_m, 0.4 Pa μmol^{-1} m^2 s; Γ^*, 3.74 Pa. Note: The negative root of the branch opening left and the positive root of the branch opening right of A_p for $\alpha = 0$ are overlaid with its oblique asymptote

For $A_c = A_j$,

$$C_{i1}^{cj} = C_{c1}^{cj} + r_m A_{c1}^{cj} \quad \text{and} \quad A_{i1}^{cj} = A_{c1}^{cj}, \tag{14a, 14b}$$

$$C_{i2}^{cj} = C_{c2}^{cj} + r_m A_{c2}^{cj} \quad \text{and} \quad A_{i2}^{cj} = A_{c2}^{cj} \tag{15a, 15b}$$

for $A_j = A_p$,

$$C_{i1}^{jp} = C_{c1}^{jp} + r_m A_{c1}^{jp} \quad \text{and} \quad A_{i1}^{jp} = A_{c1}^{jp} \tag{16a, 16b}$$

$$C_{i2}^{jp} = C_{c2}^{jp} + r_m A_{c2}^{jp} \quad \text{and} \quad A_{i2}^{jp} = A_{c2}^{jp} \tag{17a, 17b}$$

and for $A_c = A_p$,

$$C_{i1}^{cp} = C_{c1}^{cp} + r_m A_{c1}^{cp} \quad \text{and} \quad A_{i1}^{cp} = A_{c1}^{cp} \tag{18a, 18b}$$

$$C_{i2}^{cp} = C_{c2}^{cp} + r_m A_{c2}^{cp} \quad \text{and} \quad A_{i2}^{cp} = A_{c2}^{cp} \tag{19a, 19b}$$

The above solutions could be further extended to include the stomatal resistance to CO_2 diffusion ($r_s = 1/g_s$) in A_c, A_j and A_p (see Appendix 2). Figure 2 summarises the changes in the transition points in the first and fourth quadrants of the Cartesian coordinate system when the resistance(s) to CO_2 diffusion is included in the net CO_2 assimilation rate curves. For the sake of clarity, only A_c and A_j are shown.

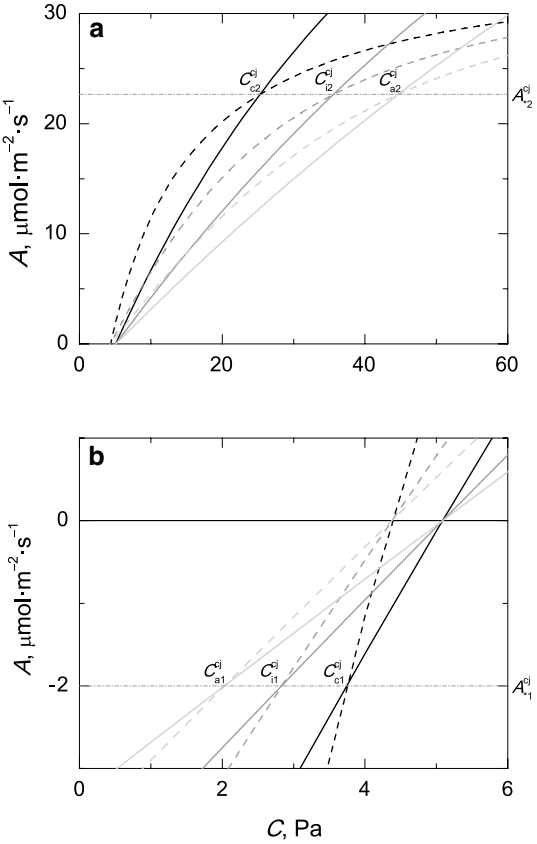

Fig. 2 Transition points $\left(C^{cj}_{*2}, A^{cj}_{*2}\right)$ and $\left(C^{cj}_{*1}, A^{cj}_{*1}\right)$ between A_c (solid lines) and A_j (dashed lines) for the rectangular and non-rectangular hyperbolic equations of the FvCB model for C_3 plants in the first (**a**) and fourth (**b**) quadrants of the Cartesian coordinate system. In the transition points, the obtained values for the net CO_2 assimilation rate (A^{cj}_{*1} and A^{cj}_{*2}) remain constant (dotted-dashed lines), while the values for the CO_2 concentration (C^{cj}_{*1} and C^{cj}_{*2}) at the transition points depend on the type of A/C rate curve (A/C_c, black lines; A/C_i, grey lines; and A/C_a, light grey lines). The asterisks stand for the CO_2 concentration at the carboxylation site (**c**), intercellular space (i) or the atmosphere (**a**). The simulation was performed using the following values for the biochemical parameters: V_{cmax}, 100 μmol m^{-2} s^{-1}; J, 150 μmol m^{-2} s^{-1}; R_d, 2 μmol m^{-2} s^{-1}; r_m, 0.45 Pa μmol^{-1} m^2 s; r_s, 0.4 Pa μmol^{-1} m^2 s; K_{co}, 62.1 Pa; Γ^*, 3.74 Pa

The analytical values for the assimilation rates (A^{xy}_{*1} and A^{xy}_{*2}) at the transition points remain constant, while the values for the CO_2 concentration increase in the first quadrant (and decrease in the fourth quadrant) when the resistance(s) to CO_2 diffusion increases. The solution $(\Gamma^*, -R_d)$ for the transition point $(C^{xy}_{c1}, A^{xy}_{c1})$ is restricted to the fourth quadrant of the Cartesian coordinate system when the rectangular hyperbolae (Eqs. 2–4) of the basic FvCB model are used. However, it should not be surprising to find out this analytical transition point $(C^{xy}_{i1}, A^{xy}_{i1})$ in the third quadrant under conditions for which $R_d r_m > \Gamma^*$ when dealing with the quadratic equations of the FvCB model.

In the mathematical analysis, it can be observed that the common transition point $(C^{xy}_{i1}, A^{xy}_{i1})$ between the three states c, j and p is always present; in contrast, the transition points $(C^{xy}_{i2}, A^{xy}_{i2})$ depend on the biochemical parameters and might not be present in the net CO_2 assimilation rate curves. Two limiting conditions can now be investigated in order to analyse all the possible combinations between the transition points between A_c, A_j and A_p regardless of the value of r_m. One is that C^{xy}_{i2} approaches C^{xy}_{i1} (i.e. $C^{xy}_{i2\to1}$) and another is that C^{xy}_{i2} approaches infinity (i.e. $C^{xy}_{i2\to\infty}$). The equation $C^{xy}_{i1} = C^{xy}_{i2}$ has to be solved for the analysis of the first limiting condition, whereas only the values for the

denominator of the first summand (i.e. C_{c2}^{xy}) of C_{i2}^{xy} (Eqs. 15a–19a) have to be inspected to analyse the second limiting condition. In the analysis, the constraint $K_{co} > 2\Gamma^*$ is imposed based on the values reported for C_3 plants (von Caemmerer 2000); consequently, there are no finite values for the biochemical parameters of the second summand (i.e. $r_m A_{c2}^{xy}$) of C_{i2}^{xy} (Eqs. 15a–19a) that can make this summand approach infinity.

The ratios between the biochemical parameters to reach the above limiting conditions for the rectangular equations of an A/C_c rate curve (i.e. $C_{c2\to1}^{xy}$ and $C_{c2\to\infty}^{xy}$) can be derived straightforward from Eqs. 5a–10a. The results are as follows:

For $C_{c2\to1}^{cj}$ and $C_{c2\to\infty}^{cj}$, respectively,

$$V_{cmax} = \frac{J\left(K_{co} + \Gamma^*\right)}{12\Gamma^*} \quad \text{and} \quad V_{cmax} = \frac{J}{4} \tag{20a, 20b}$$

for $C_{c2\to1}^{jp}$ and $C_{c2\to\infty}^{jp}$, respectively,

$$J = -\frac{12T_p}{\alpha} \quad \text{and} \quad J = 12T_p \tag{21a, 21b}$$

and for $C_{c2\to1}^{cp}$ and $C_{c2\to\infty}^{cp}$, respectively,

$$V_{cmax} = -\frac{T_p\left(K_{co} + \Gamma^*\right)}{\alpha\Gamma^*} \quad \text{and} \quad V_{cmax} = 3T_p \tag{22a, 22b}$$

Among the above ratios (Eqs. 20a–22b), the ratios between the biochemical parameters for $C_{c2\to1}^{jp}$ and $C_{c2\to1}^{cp}$ are of non-biochemical significance. They imply that there should be conditions for which one could expect triose phosphate import to chloroplasts (i.e. $T_p < 0$). In fact, if these transition points are analysed, particularly, in a non-rectangular A/C_i rate curve, one can observe that both transitions, $(C_{i1}^{cp}, A_{i1}^{cp})$ and $(C_{i1}^{jp}, A_{i1}^{jp})$, occur with the negative root of the hyperbolic branch opening left of A_p, for which the C_i domain is not applicable as indicated above. (Further details are given in Fig. S1 of Online Resource.)

When the rest of the ratios between the biochemical parameters are now investigated in the non-rectangular hyperbola equations of the FvCB model—where r_m is finite, $0 < r_m < \infty$—two solutions are in fact found for any equation like $C_{i2}^{xy} = C_{i1}^{xy}$, of which only one also fulfils the condition $A_{i2}^{xy} = A_{i1}^{xy}$ (data not shown). The analysis indeed shows that the correct ratios between the biochemical parameters for $C_{i2\to1}^{xy}$ and $C_{i2\to\infty}^{xy}$ are the same as those found for $C_{c2\to1}^{xy}$ and $C_{c2\to\infty}^{xy}$ (Eqs. 20a–22b). This means that the ratios between the biochemical parameters in the two limiting conditions do not depend on the value of r_m. The limiting conditions for the transition points can therefore be reduced as follows:

$$V_{cmax} = \frac{J\left(K_{co} + \Gamma^*\right)}{12\Gamma^*}, \tag{23}$$

$$J = 4V_{cmax}, \quad \text{and} \tag{24}$$

$$J = 12T_p \tag{25}$$

The graphic representation of A_c, A_j and A_p for A/C_i rate curves shows, firstly, that there are no experimental ratios for the biochemical parameter for which A_p (with $T_p > 0$) can be the only limitation state along the domain $\Gamma^* - r_m R_d < C_i < \infty$ and, secondly, there are ratios between the biochemical parameters for which A_c or A_j can be the only limitation state along the domain $\Gamma^* - r_m R_d < C_i < \infty$ (Fig. 3a, b). Additional ratios between the biochemical parameters can be found for which there are one or two transition points in the first quadrant of Cartesian coordinate system

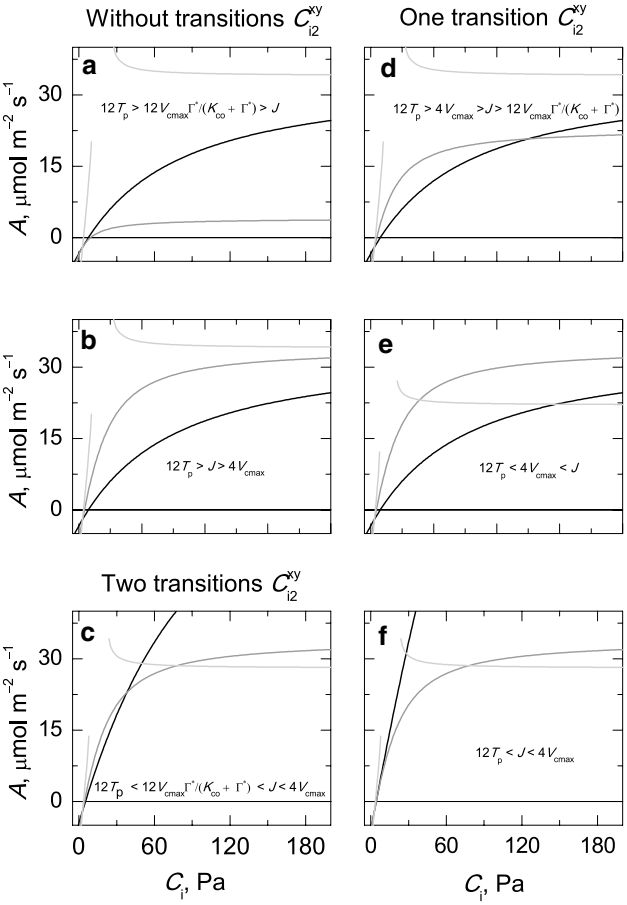

Fig. 3 Ratios between the limiting values of the biochemical parameters of a representative A/C_i rate curve, where the summation of resistances to CO_2 diffusion is included (i.e. $0 < r_m < \infty$), for which there are no transition points between the three states c, j and p (**a**, **b**) and two transition points (**c**) or there is only one transition point (**d**–**f**) in the first quadrant of the Cartesian coordinate system (C_{i2}^{xy},A_{i2}^{xy}). The symbols x and y stand for any of the three limitation states c, j and p. The simulation was performed using the following values for the biochemical parameters: V_{cmax}, 36–100 µmol m^{-2} s^{-1}; J, 24–144 µmol m^{-2} s^{-1}; T_p, 8–12 µmol m^{-2} s^{-1}; R_d, 2 µmol m^{-2} s^{-1}; r_m, 0.4 Pa µmol^{-1} m^2 s; K_{co}, 62.1 Pa; Γ^*, 3.74 Pa

(Fig. 3c–f). The latter ratios are equivalent to those discussed before for A/C_c rate curves (Gu et al. 2010). Regardless of the number of transition points (0, 1 or 2) that the ratios of the biochemical parameters can yield between the three limitation states in the first quadrant of the Cartesian coordinate system, the transition points in the fourth (or third) quadrant are always present.

3.4 Analysis of the Inhibition of the Net CO_2 Assimilation Rate at High CO_2 Concentrations

If the steady-state FvCB model is strictly followed, one can state, first, that the slopes of the oblique asymptotes of the non-rectangular hyperbolae only depend on $g_m = 1/r_m$, while the slopes of the horizontal asymptotes of A_c, A_j and A_p remain unchanged regardless of the value for g_m (Eqs. 11a–13b) and, second, the slopes of the bisecting lines (Table 2) of A_c, A_j and A_p correspond with the angle (or the perpendicular angle) of the rotation of the coordinate system that makes the summation of the coefficients of C_i^2 equal to zero (Eqs. A11 and A12). This means that there are *no* mathematical solutions for the quadratic equations of A_c, A_j and A_p (Eqs. A8–A10) in the FvCB model for which the slopes of the horizontal asymptotes can be modified to reach negative values. The fraction of glycerate ($\alpha \neq 0$) that does not return to chloroplasts through the photorespiratory cycle (Harley and Sharkey 1991) makes A_p decrease as C_i increases, but the slope of the horizontal asymptote of A_p remains unchanged, no matter what value α ($0 \leq \alpha \leq 1$) has. This indicates that A_p must finally reach a constant value as C_i increases. This conclusion also applies to the extended FvCB model described in the study by Busch et al. (2018), where the parameter α of the basic FvCB model is replaced with two new parameters α_G and α_S that stand for the proportion of glycolate carbon taken out of the photorespiratory pathway as glycine, and the proportion taken out as serine, respectively. Although α_G and α_S might not be constant and depend on the photorespiratory pathway and the reduction of supplied nitrate (Busch et al. 2018), the new equations for the three limitation states remain, from a mathematical point of view, as rectangular hyperbolae with horizontal asymptotes equivalent to those summarised in Table 2. Likewise, the extension of the FvCB model using r_m as a flux-weighted quantity that depends on mitochondrial respiration and photorespiration effects does not explain the inhibition of A/C_i at high C_i either (Tholen et al. 2012).

Despite what has been said above, there are lines of experimental evidence that indicate that negative slopes can be indeed observed in A/C_i rate curves. Woo and Wong (1983) showed that supraoptimal CO_2 concentrations inhibited the net CO_2 assimilation in cotton plants, and they proposed that an acidification mechanism mediated by CO_2 could affect both the thylakoid electron transport and the activity of key enzymes of the Calvin–Benson–Bassham cycle (Kaiser and Heber 1983; Ögren and Evans 1993). At this point, one could speculate on some mathematical explanations for negative slopes in experimental A/C_i rate curves. In the first place, one could wonder whether other rotation of the coordinates—different from the one that yields Eqs. A28 and A29—would be possible under steady-state conditions, which rendered negative asymptotes instead of horizontal asymptotes. If this were

possible, the summation of the coefficients of C_i^2 (Eqs. A11 and A12) would not be zero and so the chosen fitting method should start from extended quadratic equations as Eqs. A6 and A7, where at least four parameters defining the hyperbola equation and an angle of rotation had to be determined. In this case, the angle of rotation should depend on g_m together with other biochemical parameters. Alternatively, one could wonder whether the steady-state conditions do not hold along the whole C_i domain, particularly at supraoptimal CO_2 concentrations. If this were the case, one can assert that the equation $A = (C_i - C_c)/r_m$ is not always valid. So, A decreases at supraoptimal CO_2 concentrations because either r_m is not only diffusional and so it increases as C_i increases (Flexas et al. 2007) or the photosynthetic activity is indeed inhibited by CO_2 acidification (Kaiser and Heber 1983; Ögren and Evans 1993; Woo and Wong 1983). Reliable nonlinear fittings of A_c and A_j of the FvCB model can thus be possibly obtained under steady-state conditions using standard approaches (Duursma 2015; Gu et al. 2010; Sharkey 2016; Su et al. 2009); however, the use supraoptimal CO_2 concentrations to fit A_p might cast doubts on the fitted biochemical parameters if evidence for negative slopes in the experimental A/C_i rate curves is observed. Based on the variation of g_m with C_i (Flexas et al. 2007), other nonlinear fitting approaches proposed the combination of gas exchange methods with chlorophyll fluorescence-based methods to estimate g_m by using only data within the j state (Yin and Struik 2009).

4 Conclusions

The analysis of the steady-state FvCB model for C_3 plants starting from the standard equations of hyperbolae after rotating the coordinate system has disclosed some features hidden in the quadratic equations of A_c, A_j and A_p of the A/C_i rate curves. In particular, academic interest has been the angle of the rotation of the coordinate system from which it has been established that the oblique asymptotes of the three limitation rate curves share a common slope whose value depends only on g_m. A_p always has an oblique asymptote regardless of the value of α. The limiting conditions for the transition points in the FvCB model do not depend on g_m. The hyperbola equations of A_c, A_j and A_p in the FvCB model or in some of the extended steady-state FvCB models here discussed can only provide horizontal asymptotes when the CO_2 concentration approaches infinity when, in contrast, there is experimental evidence for negative slopes in A/C_i rate curves at high CO_2 concentrations. This leads us to the conclusion that extended quadratic equations containing a C_i^2 term might be required for the analysis of A_c, A_j and A_p or, in contrast, that steady-state conditions do not hold, particularly, with increased CO_2 concentrations. Dynamic modelling taking into account the decrease in the values for g_m or the activity inhibition of key enzymes of the Calvin–Benson–Bassham cycle by CO_2 acidification could alternatively provide suitable models for the estimation of the biochemical parameters from leaf photosynthesis.

Acknowledgements This study was funded by the Spanish National Research, Development and Innovation Plan of the Ministry of Economy and Competitiveness (Grant Numbers AGL2013-41363-R,

AGL2016-79589-R). ELM-B received a predoctoral contract from the Junta de Castilla y León (E-37-2017-0066125).

Compliance with Ethical Standards

Conflict of interest The authors declare that they have no conflict of interest.

Appendix 1

The equation of a hyperbola in standard form is as follows:

$$\frac{(\dot{x}-h)^2}{a^2}-\frac{(\dot{y}-k)^2}{b^2}=1, \quad \text{when it opens left and right or} \tag{A1}$$

$$\frac{(\dot{y}-k)^2}{b^2}-\frac{(\dot{x}-h)^2}{a^2}=1, \quad \text{when it opens upwards and downwards} \tag{A2}$$

For each hyperbola, there are two asymptotes with slopes of $\pm b/a$ forming an angle θ whose value is:

$$\theta=\arctan\left|\frac{2ab}{a^2-b^2}\right| \tag{A3}$$

The anticlockwise rotation of the coordinates by an angle β, where

$$\dot{x}=x\cos\beta+y\sin\beta, \quad \text{and} \tag{A4}$$

$$\dot{y}=-x\sin\beta+y\cos\beta, \tag{A5}$$

yields:

$$y_{\mathrm{LR}}^2+y_{\mathrm{LR}}\frac{\left(2a^2\cos\beta\sin\beta+2b^2\cos\beta\sin\beta\right)x+2a^2k\cos\beta-2b^2h\sin\beta}{b^2\sin^2\beta-a^2\cos^2\beta} + \frac{\left(b^2\cos^2\beta-a^2\sin^2\beta\right)x^2-(2b^2h\cos\beta+2a^2k\sin\beta)x+b^2h^2-a^2k^2-a^2b^2}{b^2\sin^2\beta-a^2\cos^2\beta}=0 \tag{A6}$$

and

$$y_{\mathrm{UD}}^2 + y_{\mathrm{UD}} \frac{\left(2a^2 \cos\beta \sin\beta + 2b^2 \cos\beta \sin\beta\right)x + 2a^2 k \cos\beta - 2b^2 h \sin\beta}{b^2 \sin^2\beta - a^2 \cos^2\beta} + \frac{\left(b^2 \cos^2\beta - a^2 \sin^2\beta\right)x^2 - (2b^2 h \cos\beta + 2a^2 k \sin\beta)x + b^2 h^2 - a^2 k^2 + a^2 b^2}{b^2 \sin^2\beta - a^2 \cos^2\beta} = 0, \tag{A7}$$

where LR and UD stand for hyperbolae opening left and right, and upwards and downwards, respectively. The only difference between the left-hand sides of Eqs. A6 and A7 is the sign of the term a^2b^2 in the numerator of the last coefficient. The above quadratic equations for non-rectangular hyperbolae opening left and right or upwards and downwards can now be compared, coefficient by coefficient, with each of the quadratic equations of the A/C_i rate curves of the three states c, j and p of the steady-state FvCB model. After the substitution of C_c with $C_\mathrm{i} - r_\mathrm{m}A$ in Eqs. 2–4, the new A_c, A_j and A_p are as follows:

$$A_\mathrm{c}^2 - A_\mathrm{c}\left(\frac{C_\mathrm{i} + K_\mathrm{co}}{r_\mathrm{m}} + V_\mathrm{cmax} - R_\mathrm{d}\right) + \frac{\left(V_\mathrm{cmax} - R_\mathrm{d}\right)C_\mathrm{i}}{r_\mathrm{m}} - \frac{V_\mathrm{cmax}\Gamma^* + R_\mathrm{d}K_\mathrm{co}}{r_\mathrm{m}} = 0, \tag{A8}$$

$$A_\mathrm{j}^2 - A_\mathrm{j}\left(\frac{C_\mathrm{i} + 2\Gamma^*}{r_\mathrm{m}} + J/4 - R_\mathrm{d}\right) + \frac{\left(J/4 - R_\mathrm{d}\right)C_\mathrm{i}}{r_\mathrm{m}} - \frac{\left(J/4 + 2R_\mathrm{d}\right)\Gamma^*}{r_\mathrm{m}} = 0, \quad \text{and} \tag{A9}$$

$$A_\mathrm{p}^2 - A_\mathrm{p}\left(\frac{C_\mathrm{i} - (1+3\alpha)\Gamma^*}{r_\mathrm{m}} + 3T_\mathrm{p} - R_\mathrm{d}\right) + \frac{\left(3T_\mathrm{p} - R_\mathrm{d}\right)C_\mathrm{i}}{r_\mathrm{m}} - \frac{\left(3T_\mathrm{p} - R_\mathrm{d}\right)\Gamma^*}{r_\mathrm{m}} = 0 \tag{A10}$$

In the first instance, it is observed that the summation of the coefficients of C_i^2 in each of the three rate curves is zero (Eqs. A8–A10). Therefore, the rotation of the coordinates has to fulfil the condition:

$$b^2 \cos^2\beta - a^2 \sin^2\beta = 0, \quad \text{and so} \tag{A11}$$

$$\beta = \pm \arctan\frac{b}{a} + n\pi, \quad \text{where } n = 0, 1, 2, \ldots \tag{A12}$$

This implies that one of the two asymptotes of A_c, A_j and A_p is now parallel to the horizontal axis of the Cartesian coordinate system (i.e. the slope $m_{\mathrm{asy1}} = 0$). Because the rotation does not change the angle between the two asymptotes of the hyperbolae (Eq. A3), θ remains constant and so the slope of the second asymptote (m_{asy2}) has to be as follows:

$$m_{asy2} = \pm 2ab \big/ \left(a^2 - b^2\right) \tag{A13}$$

The rotation of the coordinates was chosen to be anticlockwise and so the positive value only applies here. The slopes m_{asy1} and m_{asy2} will be renamed m_{asyn} and m_{asyp}, respectively, after the rotation of the coordinates (see below). Figure 4 summarises the

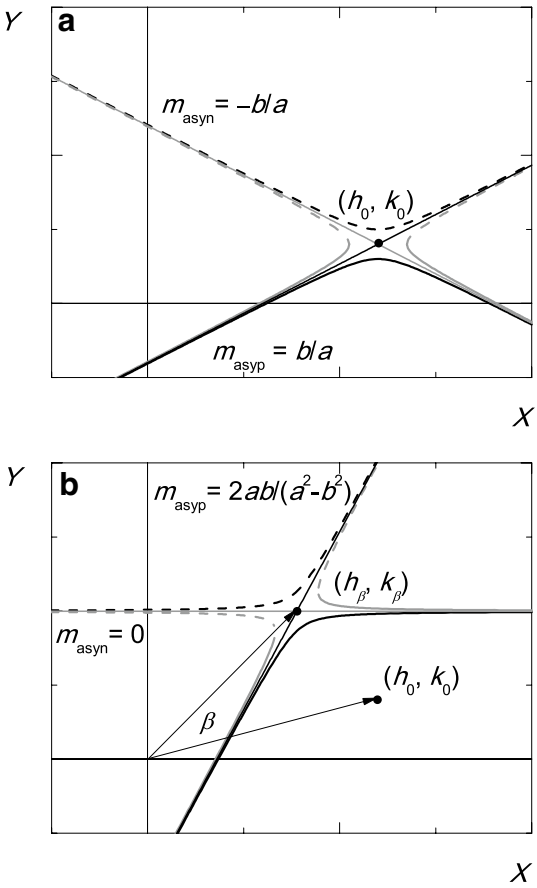

Fig. 4 Hyperbolae opening upwards and downwards (thick black lines) and left and right (thick grey lines) in standard form (**a**) and after a rotation of the coordinates by an angle β (**b**) together with their positive (thin black line) and negative (thin grey line) asymptotes and their respective centres (black dots). The angle of rotation β was chosen to be equal to b/a and so to fulfil one of the conditions of the quadratic equations of A_c, A_j and A_p of the (non)-rectangular hyperbolic FvCB model for C_3 plants. A_c and A_j are rotated hyperbolae opening upwards and downwards, while A_p opens left and right (see text for further details)

main changes in the graphic representation of the two types of hyperbolae and their asymptotes after the rotation of the coordinates.

In the second instance, A_c, A_j and A_p share a common term within the second coefficient of the quadratic equations of A_c, A_j and A_p (i.e. C_i/r_m). This implies that for the three equations, the following equality holds:

$$\frac{2a^2 \cos\beta \sin\beta + 2b^2 \cos\beta \sin\beta}{b^2 \sin^2\beta - a^2 \cos^2\beta} = -\frac{1}{r_m} \tag{A14}$$

The anticlockwise rotation of the coordinates by $\beta = \arctan b/a + n\pi$, where $n = 0$, yields:

$$\frac{2ab}{a^2 - b^2} = \frac{1}{r_m} \tag{A15}$$

This solution indicates that the oblique asymptotes of three A_c, A_j and A_p rate curves have in common their slope, which results equal to the mesophyll conductance to CO_2 diffusion ($g_m = 1/r_m$).

In the third instance, the second coefficient of each quadratic rate curve is in fact the negative value of the sum of its two asymptotes. If Eqs. A4 and A5 are applied to both the negative and positive asymptotes of the standard forms of the hyperbolae (Eqs. A1 and A2), the following equations are obtained:

$$y_{asyn} = \frac{ak + bh}{a\cos\beta + b\sin\beta} + \frac{a\sin\beta - b\cos\beta}{a\cos\beta + b\sin\beta}x = n_{asyn} + m_{asyn}x, \quad \text{and} \tag{A16}$$

$$y_{asyp} = \frac{ak - bh}{a\cos\beta - b\sin\beta} + \frac{a\sin\beta + b\cos\beta}{a\cos\beta - b\sin\beta}x = n_{asyp} + m_{asyp}x, \tag{A17}$$

where y_{asyn} and y_{asyp} stand for the new asymptotes after the rotation of the coordinates by β (Fig. 4). The sum of the asymptotes is equal to the negative value of the summation of the coefficients of y_{LR} and y_{UD} in Eqs. A6 and A7:

$$y_{asyn} + y_{asyp} = -\frac{\left(2a^2\cos\beta\sin\beta + 2b^2\cos\beta\sin\beta\right)x + 2a^2k\cos\beta - 2b^2h\sin\beta}{b^2\sin^2\beta - a^2\cos^2\beta} \tag{A18}$$

If, particularly, $\beta = \arctan b/a$, then the slopes have the following values in Eqs. A16 and A17: $m_{asyn} = 0$ and $m_{asyp} = 2ab/(a^2 - b^2)$. So now we can rewrite the second coefficients of the A_c, A_j and A_p rate curves as follows:

$$y^c_{asyn} + y^c_{asyp} = \frac{C_i + K_{co}}{r_m} + V_{cmax} - R_d \tag{A19}$$

$$y^j_{asyn} + y^j_{asyp} = \frac{C_i + 2\Gamma^*}{r_m} + J/4 - R_d \tag{A20}$$

$$y^p_{asyn} + y^p_{asyp} = \frac{C_i - (1 + 3\alpha)\Gamma^*}{r_m} + 3T_p - R_d, \tag{A21}$$

where the superscript indicates the name of the states c, j or p.

In order to know individually the equations for each of the two asymptotes of A_c, A_j and A_p, one can derive the values of the negative asymptotes (y_{asyn}) from the term that multiplies x in the third coefficient of the quadratic equations (Eqs. A6 and A7). This term is, in fact, the negative value of the product between Eqs. A14 and A16, when $m_{asyn} = 0$. Therefore, Eqs. A19–A21 can now be split as follows:

$$y^c_{asyp} = \frac{C_i + K_{co}}{r_m} \quad \text{and} \tag{A22}$$

$$y_{\text{asyn}}^{\text{c}} = V_{\text{cmax}} - R_{\text{d}}, \tag{A23}$$

$$y_{\text{asyp}}^{\text{j}} = \frac{C_{\text{i}} + 2\Gamma^*}{r_{\text{m}}} \quad \text{and} \tag{A24}$$

$$y_{\text{asyn}}^{\text{j}} = J/4 - R_{\text{d}}, \quad \text{and} \tag{A25}$$

$$y_{\text{asyp}}^{\text{p}} = \frac{C_{\text{i}} - (1+3\alpha)\Gamma^*}{r_{\text{m}}} \quad \text{and} \tag{A26}$$

$$y_{\text{asyn}}^{\text{p}} = 3T_{\text{p}} - R_{\text{d}}. \tag{A27}$$

The intersection between the oblique and horizontal asymptotes can be used to know the centre of the hyperbolae. The slopes of the bisecting lines are as follows:

$$m_{\text{bis}}^{\text{x}} = -r_{\text{m}} - \sqrt{1 + r_{\text{m}}^2}, \quad \text{where } x \text{ stands for c } or \text{ j, and} \tag{A28}$$

$$m_{\text{bis}}^{\text{p}} = -r_{\text{m}} + \sqrt{1 + r_{\text{m}}^2} \tag{A29}$$

The vertices of each hyperbola can also be derived from the intersections between the equation of the bisecting line—passing through the vertices and the centre of the hyperbola—and the corresponding quadratic equation (Eqs. A8–A10). Table 2 includes a summary of the equations and values that describe the rectangular and non-rectangular hyperbolic equations of the FvCB model.

Appendix 2

Under steady-state conditions, the net CO_2 assimilation rate can also be obtained as $A = (C_{\text{a}} - C_{\text{i}})/r_{\text{s}}$, where $r_{\text{s}} = 1/g_{\text{s}}$, if particularly the transpiration rate (E) is considered negligible and consequently $g_{\text{s}} \pm E/2 \approx g_{\text{s}}$ (Farquhar and Sharkey 1982). The transition points for the new equations in A/C_{a} rate curves, when both r_{m} and r_{s} are grouped together in the analysis, are now as follows:

For $A_{\text{c}} = A_{\text{j}}$,

$$C_{\text{a1}}^{\text{cj}} = C_{\text{c1}}^{\text{cj}} + (r_{\text{s}} + r_{\text{m}})A_{\text{c1}}^{\text{cj}} \quad \text{and} \quad A_{\text{a1}}^{\text{cj}} = A_{\text{c1}}^{\text{cj}} \tag{A30a, A30b}$$

$$C_{\text{a2}}^{\text{cj}} = C_{\text{c2}}^{\text{cj}} + (r_{\text{s}} + r_{\text{m}})A_{\text{c2}}^{\text{cj}} \quad \text{and} \quad A_{\text{a2}}^{\text{cj}} = A_{\text{c2}}^{\text{cj}} \tag{A31a, A31b}$$

for $A_{\text{j}} = A_{\text{p}}$,

$$C_{a1}^{jp} = C_{c1}^{jp} + (r_s + r_m)A_{c1}^{jp} \quad \text{and} \quad A_{a1}^{jp} = A_{c1}^{jp} \qquad \text{(A32a, A32b)}$$

$$C_{a2}^{jp} = C_{c2}^{jp} + (r_s + r_m)A_{c2}^{jp} \quad \text{and} \quad A_{a2}^{jp} = A_{c2}^{jp} \qquad \text{(A33a, A33b)}$$

and for $A_c = A_p$,

$$C_{a1}^{cp} = C_{c1}^{cp} + (r_s + r_m)A_{c1}^{cp} \quad \text{and} \quad A_{a1}^{cp} = A_{c1}^{cp} \qquad \text{(A34a, A34b)}$$

$$C_{a2}^{cp} = C_{c2}^{cp} + (r_s + r_m)A_{c2}^{cp} \quad \text{and} \quad A_{a2}^{cp} = A_{c2}^{cp} \qquad \text{(A35a, A35b)}$$

References

Bellasio C (2019) A generalised dynamic model of leaf-level C_3 photosynthesis combining light and dark reactions with stomatal behaviour. Photosynth Res 141:99–118. https://doi.org/10.1007/s11120-018-0601-1

Bellasio C, Beerling DJ, Griffiths H (2016) Deriving C_4 photosynthetic parameters from combined gas exchange and chlorophyll fluorescence using an Excel tool: theory and practice. Plant Cell Environ 39:1164–1179. https://doi.org/10.1111/pce.12626

Buckley TN (2017) Modeling stomatal conductance. Plant Physiol 174:572–582. https://doi.org/10.1104/pp.16.01772

Busch FA, Sage RF, Farquhar GD (2018) Plants increase CO_2 uptake by assimilating nitrogen via the photorespiratory pathway. Nat Plants 4:46–54. https://doi.org/10.1038/s41477-017-0065-x

Duursma RA (2015) Plantecophys: an R package for analysing and modelling leaf gas exchange data. PLoS One. https://doi.org/10.1371/journal.pone.0143346

Ethier GJ, Livingston NJ (2004) On the need to incorporate sensitivity to CO_2 transfer conductance into the Farquhar–von Caemmerer–Berry leaf photosynthesis model. Plant Cell Environ 27:137–153. https://doi.org/10.1111/j.1365-3040.2004.01140.x

Farquhar GD, Sharkey TD (1982) Stomatal conductance and photosynthesis. Ann Rev Plant Physiol Plant Mol Biol 33:317–345. https://doi.org/10.1146/annurev.pp.33.060182.001533

Farquhar GD, Caemmerer SV, Berry JA (1980) A biochemical model of photosynthetic CO_2 assimilation in leaves of C_3 species. Planta 149:78–90. https://doi.org/10.1007/bf00386231

Flexas J, Diaz-Espejo A, Galmes J, Kaldenhoff R, Medrano H, Ribas-Carbo M (2007) Rapid variations of mesophyll conductance in response to changes in CO_2 concentration around leaves. Plant Cell Environ 30:1284–1298. https://doi.org/10.1111/j.1365-3040.2007.01700.x

Flexas J, Ribas-Carbo M, Diaz-Espejo A, Galmes J, Medrano H (2008) Mesophyll conductance to CO_2: current knowledge and future prospects. Plant Cell Environ 31:602–621. https://doi.org/10.1111/j.1365-3040.2007.01757.x

Goudriaan J (1979) Family of saturation type curves, especially in relation to photosynthesis. Ann Bot 43:783–785. https://doi.org/10.1093/oxfordjournals.aob.a085693

Gu LH, Pallardy SG, Tu K, Law BE, Wullschleger SD (2010) Reliable estimation of biochemical parameters from C_3 leaf photosynthesis-intercellular carbon dioxide response curves. Plant Cell Environ 33:1852–1874. https://doi.org/10.1111/j.1365-3040.2010.02192.x

Harley PC, Sharkey TD (1991) An improved model of C_3 photosynthesis at high CO_2: reversed O_2 sensitivity explained by lack of glycerate reentry into the chloroplast. Photosynth Res 27:169–178. https://doi.org/10.1007/BF00035838

Jahan E, Amthor JS, Farquhar GD, Trethowan R, Barbour MM (2014) Variation in mesophyll conductance among Australian wheat genotypes. Funct Plant Biol 41:568–580. https://doi.org/10.1071/fp13254

Kaiser G, Heber U (1983) Photosynthesis of leaf cell protoplasts and permeability of the plasmalemma to some solutes. Planta 157:462–470. https://doi.org/10.1007/bf00397204

Medlyn BE et al (2011) Reconciling the optimal and empirical approaches to modelling stomatal conductance. Global Change Biol 17:2134–2144. https://doi.org/10.1111/j.1365-2486.2010.02375.x

Miao ZW, Xu M, Lathrop RG, Wang YF (2009) Comparison of the A-C_c curve fitting methods in determining maximum ribulose 1·5-bisphosphate carboxylase/oxygenase carboxylation rate, potential light saturated electron transport rate and leaf dark respiration. Plant Cell Environ 32:109–122. https://doi.org/10.1111/j.1365-3040.2008.01900.x

Morales A, Kaiser E, Yin XY, Harbinson J, Molenaar J, Driever SM, Struik PC (2018) Dynamic modelling of limitations on improving leaf CO_2 assimilation under fluctuating irradiance. Plant Cell Environ 41:589–604. https://doi.org/10.1111/pce.13119

Niinemets U, Diaz-Espejo A, Flexas J, Galmes J, Warren CR (2009) Importance of mesophyll diffusion conductance in estimation of plant photosynthesis in the field. J Exp Bot 60:2271–2282. https://doi.org/10.1093/jxb/erp063

Noe SM, Giersch C (2004) A simple dynamic model of photosynthesis in oak leaves: coupling leaf conductance and photosynthetic carbon fixation by a variable intracellular CO_2 pool. Funct Plant Biol 31:1195–1204. https://doi.org/10.1071/fp03251

Ögren E, Evans JR (1993) Photosynthetic light-response curves. I. The influence of CO2 partial-pressure and leaf inversion. Planta 189:182–190. https://doi.org/10.1007/bf00195075

Price GD, Badger MR, von Caemmerer S (2011) The prospect of using cyanobacterial bicarbonate transporters to improve leaf photosynthesis in C_3 crop plants. Plant Physiol 155:20–26. https://doi.org/10.1104/pp.110.164681

Sharkey TD (1985a) O_2-insensitive photosynthesis in C_3 plants. Its occurrence and a possible explanation. Plant Physiol 78:71–75. https://doi.org/10.1104/pp.78.1.71

Sharkey TD (1985b) Photosynthesis in intact leaves of C_3 plants: physics, physiology and rate limitations. Bot Rev 51:53–105. https://doi.org/10.1007/bf02861058

Sharkey TD (2016) What gas exchange data can tell us about photosynthesis. Plant Cell Environ 39:1161–1163. https://doi.org/10.1111/pce.12641

Su YH, Zhu GF, Miao ZW, Feng Q, Chang ZQ (2009) Estimation of parameters of a biochemically based model of photosynthesis using a genetic algorithm. Plant Cell Environ 32:1710–1723. https://doi.org/10.1111/j.1365-3040.2009.02036.x

Tholen D, Ethier G, Genty B, Pepin S, Zhu XG (2012) Variable mesophyll conductance revisited: theoretical background and experimental implications. Plant Cell Environ 35:2087–2103. https://doi.org/10.1111/j.1365-3040.2012.02538.x

von Caemmerer S (2000) Biochemical models of leaf photosynthesis. CSIRO, Collingwood

von Caemmerer S (2013) Steady-state models of photosynthesis. Plant, Cell Environ 36:1617–1630. https://doi.org/10.1111/pce.12098

Wolfram Research I (2015) Mathematica, Version 10.3. Wolfram Research Inc, Champaign

Woo KC, Wong SC (1983) Inhibition of CO_2 assimilation by supraoptimal CO_2: effect of light and temperature. Aust J Plant Physiol 10:75–85. https://doi.org/10.1071/pp9830075

Wullschleger SD (1993) Biochemical limitations to carbon assimilation in C_3 plants-a retrospective analysis of the A/C_i curves from 109 species. J Exp Bot 44:907–920. https://doi.org/10.1093/jxb/44.5.907

Yin XY, Struik PC (2009) Theoretical reconsiderations when estimating the mesophyll conductance to CO_2 diffusion in leaves of C_3 plants by analysis of combined gas exchange and chlorophyll fluorescence measurements. Plant Cell Environ 32:1513–1524. https://doi.org/10.1111/j.1365-3040.2009.02016.x

Yin XY, Struik PC (2017) Simple generalisation of a mesophyll resistance model for various intracellular arrangements of chloroplasts and mitochondria in C_3 leaves. Photosynth Res 132:211–220. https://doi.org/10.1007/s11120-017-0340-8

Zeng W, Zhou GS, Jia BR, Jiang YL, Wang Y (2010) Comparison of parameters estimated from A/C_i and A/C_c curve analysis. Photosynthetica 48:323–331. https://doi.org/10.1007/s11099-010-0042-3